

# Comparison of plasma sheet dynamics during pseudobreakups and expansive aurorae

M. O. Fillingim, G. K. Parks, L. J. Chen, and M. McCarthy  
*University of Washington, Geophysics Program, Box 351650, Seattle, Washington 98195*

J. F. Spann  
*NASA Marshall Space Flight Center, Huntsville, Alabama 35812*

R. P. Lin  
*Space Sciences Laboratory, University of California, Berkeley, California 94720*

(Received 8 August 2000; accepted 5 September 2000)

Global auroral images and plasma sheet ion distributions and magnetic field data are examined for two intervals when the Ultraviolet Imager (UVI) onboard the Polar spacecraft was imaging the entire northern auroral oval and, at the same time, the Wind spacecraft was passing through the near-Earth plasma sheet. On 26 July 1997, UVI recorded a series of brief, localized auroral brightenings known as pseudobreakups. On 27 March 1996, UVI observed several global expansions of auroral activity. Large variations in the magnetic field were observed by the Wind magnetometer, large velocity moments were derived from Wind ion measurements, and ions were accelerated to mega-electron-volt energies during both types of activity. The plasma sheet dynamics appear very similar during these two different types of auroral activities. Closer inspection of the ion distribution functions and energy spectra indicate that the plasma sheet dynamics need to be characterized kinetically. © 2001 American Institute of Physics. [DOI: 10.1063/1.1355679]

## I. INTRODUCTION

From the ground, a pseudobreakup is seen as the disruption of an auroral arc other than the equatorward most arc.<sup>1</sup> The increase in auroral luminosity is localized spatially and lasts only a few minutes.<sup>2</sup> Conversely, substorm expansive phase aurorae begin in a localized region, but then the region of intense emission rapidly expands in latitude and longitude and can encompass nearly the entire nightside ionosphere. Intense auroral precipitation can last for an hour or more.<sup>2</sup>

The auroral region is linked magnetically to the distant regions of the magnetosphere and the plasma sheet, and auroral images reveal information about the dynamics that accelerate and precipitate electrons. To try to understand what physical processes in the magnetosphere are associated with these seemingly different auroral forms, we compare global images to plasma and magnetic field observations made in the near-Earth plasma sheet for two intervals. During both intervals, the Ultraviolet Imager (UVI)<sup>3</sup> onboard the Polar spacecraft was imaging the entire northern auroral region, and the Wind spacecraft was taking plasma<sup>4</sup> and magnetic field<sup>5</sup> measurements in the plasma sheet between 10 and 20 Earth radii ( $R_E$ ). During the first interval, 26 July 1997, UVI recorded a series of pseudobreakups. On 27 March 1996, UVI observed several major substorm auroral expansions.

Wind plasma and magnetic field observations are described in Sec. II. The relationship between the auroral observations and plasma sheet properties for 26 July 1997, has been briefly described earlier.<sup>6</sup> Similarly, the plasma sheet dynamics for 27 March 1996, has been discussed from a magnetohydrodynamic (MHD) fluid point of view<sup>7</sup> and from a plasma kinetic point of view.<sup>8</sup> Here we compare these two

events to further elucidate the behavior of these two auroral forms. Conclusions based on the comparison are given in Sec. III.

## II. OBSERVATIONS

In Fig. 1, we show two sequences of images taken by UVI. The first sequence, taken on 26 July 1997 (first column), has been identified as a pseudobreakup; the region of intense electron precipitation does not expand more than a few degrees in latitude or a few hours in local time and lasts only a few minutes. Compare these images with the images taken on 27 March 1996 (second column). The auroral brightening begins in a localized area, but the region of intense electron precipitation expands globally in latitude and longitude and persists for nearly an hour.

The images are in magnetic coordinates; local midnight is at the bottom. Each image has been taken with a filter that passes the Lyman–Birge–Hopfield molecular nitrogen emissions in the wavelength range from 160 to 180 nm. The intensity of the auroral emission in this wavelength range is proportional to the energy flux into the ionosphere due to precipitating electrons.<sup>9,10</sup> The integration time for each image is about 37 s. The ionospheric footprint of the Wind spacecraft is marked on each image. The footprint of the field line on which Wind was located was mapped down to the ionosphere using the semi-empirical magnetic field model of Tsyganenko.<sup>11</sup> Near 06 UT on 26 July 1997, Wind was located at  $(-11, 3, 0) R_E$ . At 14:30 UT on 27 March 1996, Wind was located near  $(-15, 7, 1) R_E$ .

Figures 2 and 3 show a summary of the auroral activity measured by UVI and of the plasma and magnetic field be-

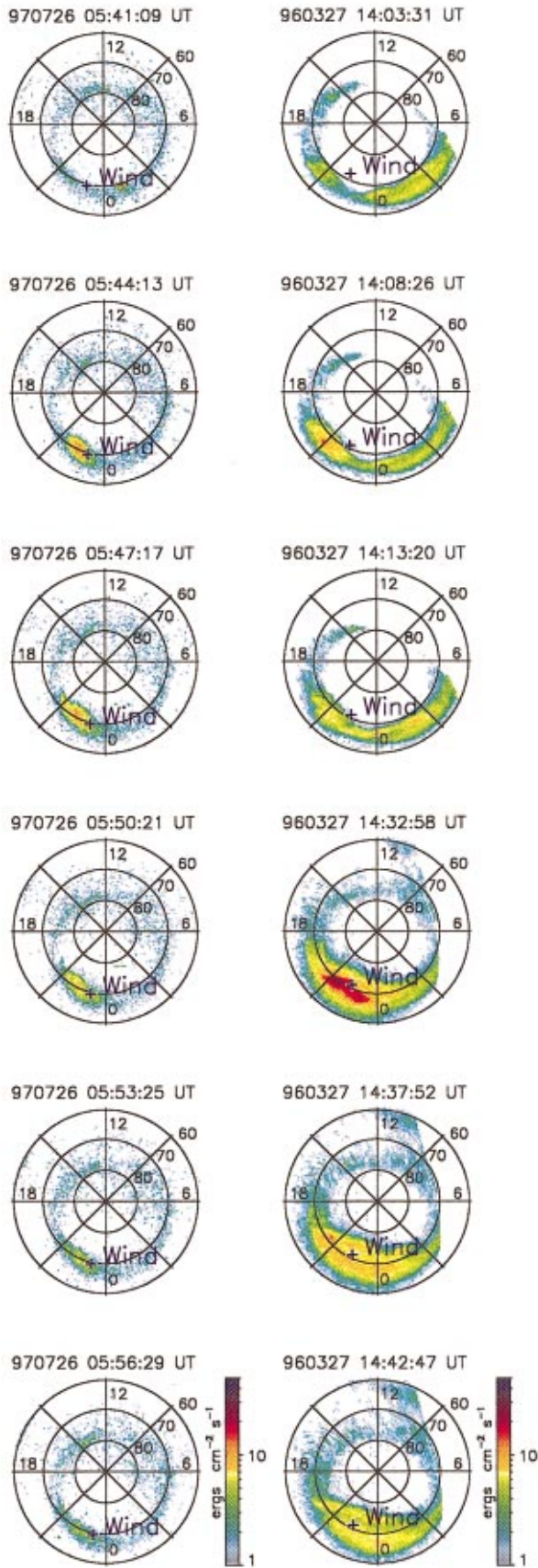


FIG. 1. (Color) Polar UVI images of a pseudobreakup (first column) and an expansive aurora (second column).

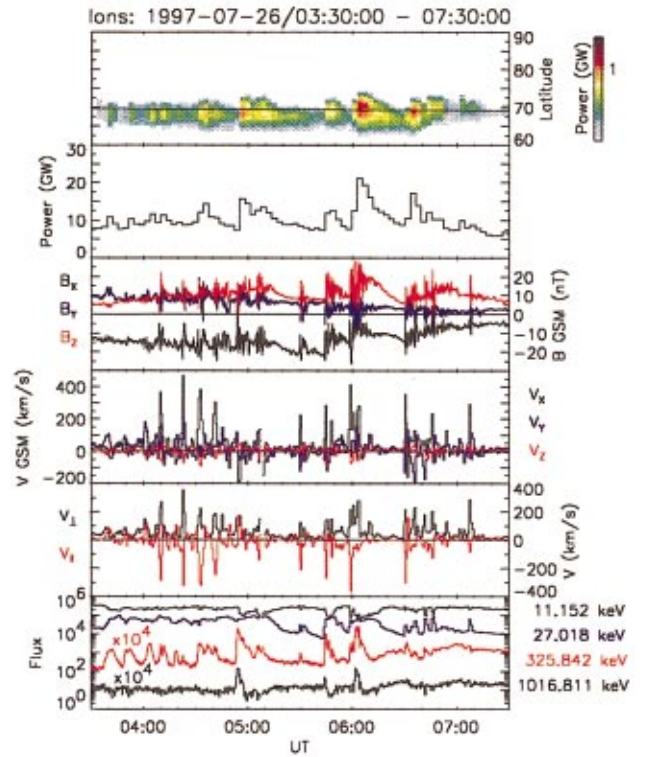


FIG. 2. (Color) From top to bottom: auroral keogram, energy deposition rate (power) from precipitating electrons (both determined from UVI images), magnetic field in GSM coordinates, ion velocity moments in GSM and magnetic field-aligned coordinates, ion omnidirectional fluxes at indicated energies (last four panels measured by Wind). The data were taken 26 July 1997.

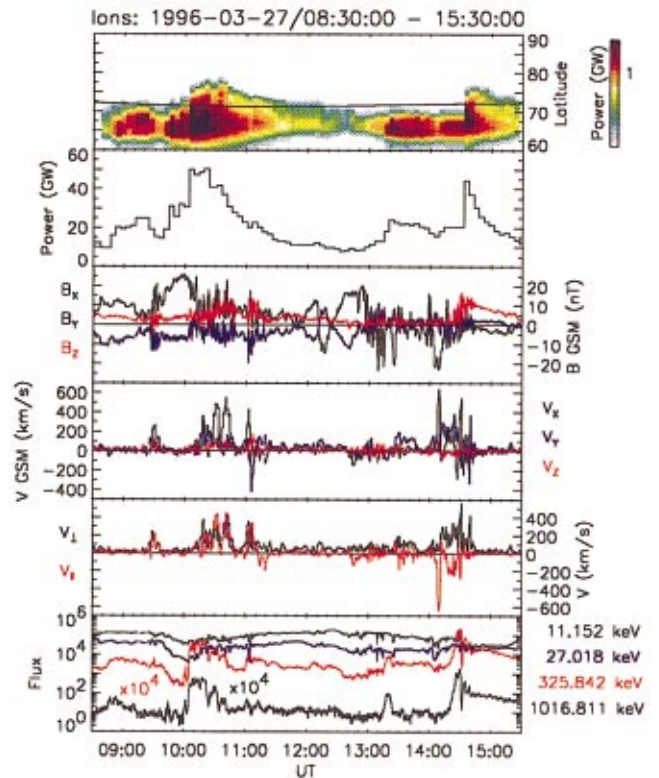


FIG. 3. (Color) Same format as Fig. 2, except that the data were taken 27 March 1996.

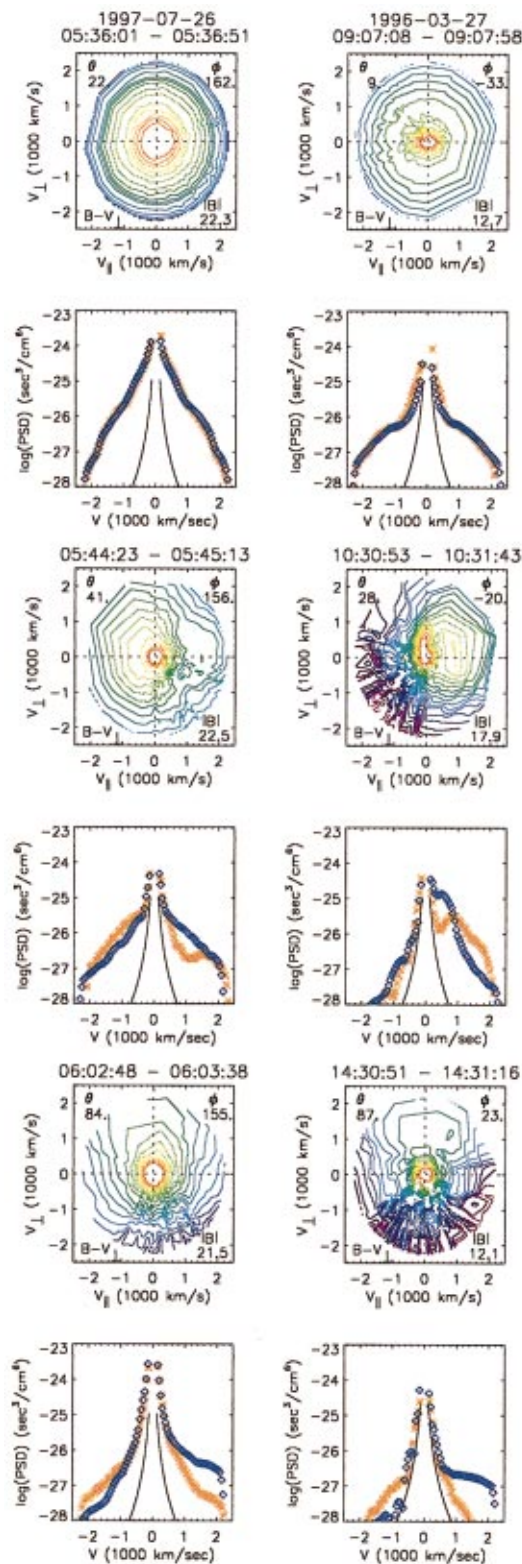


FIG. 4. (Color) First, third, and fifth rows: isocontours of ion velocity distribution functions in the  $\mathbf{B}-V_{\perp}$  plane in the spacecraft frame. Second, fourth, and sixth rows: cuts of the distribution functions in the direction parallel (orange stars) and perpendicular (blue diamonds) to the magnetic field. The smooth solid line represents the noise level of the instrument.

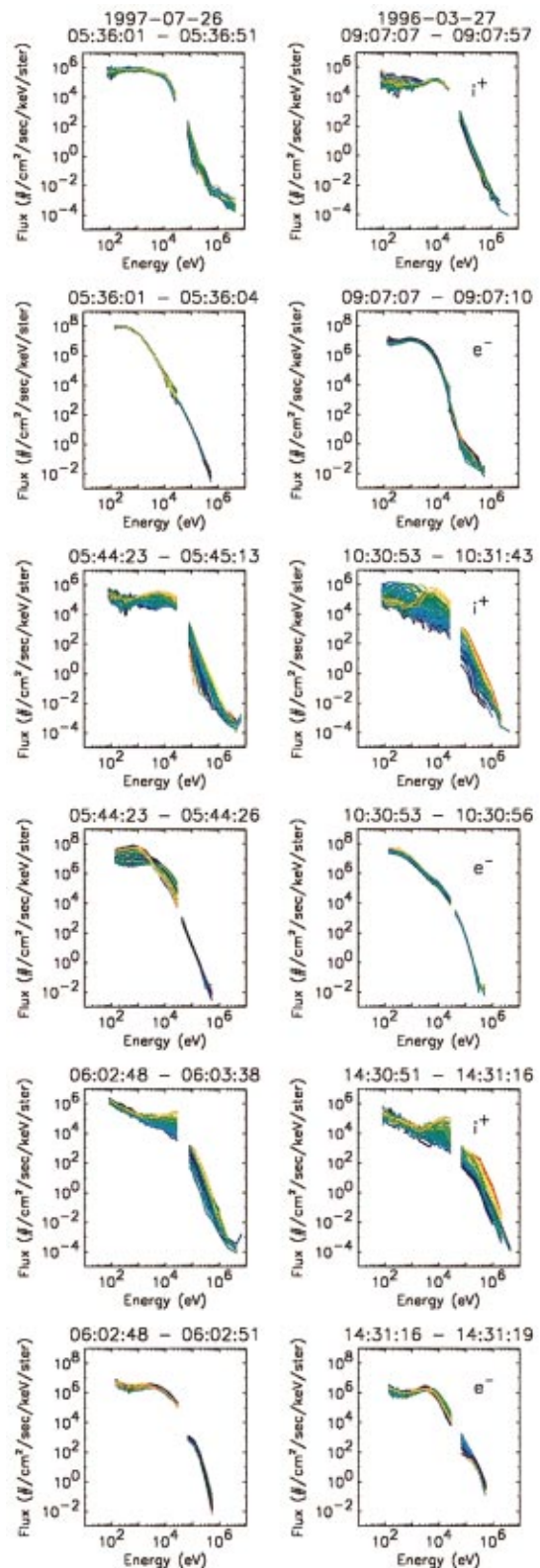


FIG. 5. (Color) First, third, and fifth rows: ion energy spectra for energies from 70 eV to 7 MeV. The color corresponds to the direction of the ion flux; red is earthward, blue is tailward. The times of the data are the same as that shown in Fig. 4. Second, fourth, and sixth rows: electron energy spectra for energies from 100 eV to 7 MeV. Red corresponds to electron flux parallel to the local magnetic field; blue is antiparallel.

havior measured in the plasma sheet by Wind for 26 July 1997, and 27 March 1996, respectively. The top panel shows the latitudinal extent of auroral activity between 21 and 03 magnetic local time in the ionosphere as a function of time. The black line is the latitude of the footprint of Wind. A measure of the energy deposition rate into the ionosphere is obtained by integrating energy flux derived from the images over area. The sum of the energy deposition rate over magnetic latitudes greater than  $60^\circ$  and over local times from 21 to 03 in gigawatts is plotted in the second panel. Three components of the 3 s resolution magnetic field data from Wind in geocentric solar magnetospheric (GSM) coordinates are displayed in the third panel. The fourth panel shows three components of the ion velocity moment,  $\langle \mathbf{v} \rangle$ , in GSM coordinates calculated from the ion distribution function. The distribution function was measured for ions with energies from 70 eV to 30 keV with a resolution of either 25 or 50 s depending upon the instrument mode. The fifth panel redisplay the ion velocity moment in magnetic field-aligned coordinates. The bottom panel shows the omnidirectional flux of ions at energies of 11, 27, and 326 keV and 1 MeV.

We note that high velocity moments occur during both types of auroral activity. During intense aurora the velocity moment is not constant at a large value; it is intermittent or bursty, hence, the term “bursty bulk flows” introduced in Ref. 12. There are periods when intense aurora are seen, but the velocity moment is small, and periods when the velocity moment is quite large, but there is no associated auroral activity. The former (see, for example, 13 to 14 UT in Fig. 3) can be explained as a matter of spacecraft location; the flux tube of the spacecraft may not be connected to the region of the ionosphere where intense aurora is occurring. However, a large increase in the ion velocity moment that is not accompanied by auroral activity (see 04:23 and 05:30 UT in Fig. 2) suggests that the communication between the plasma sheet and the ionosphere can be disrupted. MHD suggests that these large  $\langle \mathbf{v} \rangle$  are caused by  $\mathbf{E} \times \mathbf{B}$  convective flows. However, in nearly all cases shown here, a significant portion of the velocity is directed parallel to the magnetic field. (We caution the reader that the field-aligned high mean velocity recorded near 14:10 UT on 27 March 1996, is associated with a large magnitude magnetic field direction primarily in the X direction which would indicate that the spacecraft was sampling ion beams in the plasma sheet boundary layer.)

Every high velocity moment event is accompanied by relatively large amplitude, high frequency fluctuations in all three components of the magnetic field. The frequencies of these oscillations can be as high as the local ion gyrofrequency (between 0.1 and 0.3 Hz in most cases). These fluctuations imply the presence of inductive electric fields and time variations in the electric fields that cannot be ignored when discussing ion dynamics. The ion omnidirectional flux curves demonstrate that these events also efficiently energize particles up to mega-electron-volt (MeV) energies.

To better understand how the observed high  $\langle \mathbf{v} \rangle$  are produced, we examine the ion distribution functions. Figure 4 shows isocontour plots of phase space densities and cuts of the isocontour plots for some representative ion distribution functions. The first column is from 26 July 1997; the second

column is from 27 March 1996. The first, third, and fifth rows are two-dimensional slices of the full three-dimensional distribution functions in the  $\mathbf{B}-\mathbf{V}_\perp$  plane in the spacecraft frame of reference. The horizontal and vertical axes are velocities in km/s parallel and perpendicular to the magnetic field, respectively. The numbers in the upper left, upper right, and lower right are the magnetic field elevation, azimuth (both in GSM), and magnitude. The second, fourth, and sixth rows show cuts of the contour plots along the parallel (orange stars) and perpendicular (blue diamonds) directions. The horizontal axis is velocity in km/s; the vertical axis is the logarithm of the phase space density in  $\text{s}^3 \text{cm}^{-6}$ . The smooth solid lines are the instrument noise level.

The distributions in the first row represent the ion populations before the large ion velocity moment events. The contours are nearly circular, indicating isotropic distributions. The distribution from 26 July 1997, consists of a single component; the distribution from 27 March 1996, appears to consist of two components. The distributions in the third and fifth rows come from times of high velocity moment. These distributions are very anisotropic. In all cases, there is an enhancement of phase space density going toward the Earth and a reduction in the tailward direction. Strong gradients in the phase space density are apparent. The distributions in the third row have beam-like features encompassing a wide range of pitch angles. At 05:44 on 26 July 1997, the velocity moment is directed toward the upper left in a direction approximately  $135^\circ$  away from the beam. The distributions also appear to be multicomponent with a low-energy component (less than about 1 keV) responding differently than particles at higher energy. At 10:30 on 27 March 1996, there is an anisotropic core of low energy ions. The remaining three active distributions have a more isotropic and apparently stationary core of ions with energies less than 1 keV. The distributions in the fifth row both have a very hot component in the direction perpendicular to the magnetic field. The presence of a stationary core indicates that the hot component is not set into motion by an  $\mathbf{E} \times \mathbf{B}$  drift.

Another way to study the source of these particles is to examine the behavior of the differential energy spectra. Figure 5 shows examples of the ion and electron energy spectra for both 26 July 1997 (first column), and 27 March 1996 (second column). The first, third, and fifth rows contain the energy spectra for ions. For each plot there are 120 curves in the energy range from 70 eV to 30 keV corresponding to the 120 look directions of the ion (proton) electrostatic analyzer (PESA) and 40 curves in the energy range from 67 keV to 7 MeV corresponding to the 40 look directions of the ion solid state telescopes (SST). All PESA spectra are integrated over 50 s except for 14:30 on 26 March 1996, which is integrated for 25 s. All ion SST spectra are integrated over 6 s. Red colors correspond to ion fluxes in the positive X GSM direction (approximately earthward or sunward); blue colors correspond to ion fluxes in the negative X GSM direction (tailward).

The second, fourth, and sixth rows contain the energy spectra for electrons. For each plot there are 88 curves in the energy range from 100 eV to 30 keV corresponding to the 88 look directions of the electron electrostatic analyzer (EESA)

and 40 curves in the energy range from 22 keV to 7 MeV corresponding to the 40 look directions of the electron SST. All EESA spectra are integrated over 3 s. Electron SST spectra collected on 26 July 1997, are integrated over 12 s; those collected on 27 March 1996, are integrated over 6 s. The integration times of the electron spectra begin at the same time as the ion spectra above them except for 14:31 on 27 March 1996, which begins at the end of ion integration time due to lack of data. For the electrons, red colors correspond to fluxes in the direction of the local magnetic field, and blue colors correspond to fluxes in the direction opposite of the magnetic field.

The first row shows energy spectra representative of the quiet plasma sheet before a high velocity moment event. There is little spread in the curves indicating that ion fluxes in all directions are nearly equal (isotropic). Ion spectra during high velocity moment events are shown in the third and fifth rows. During these times the ion fluxes are highly anisotropic. Fluxes in the earthward direction are higher, up to two orders of magnitude, than fluxes in the tailward direction for energies higher than a few kilo-electron-volts (keV). Features in the energy spectra are directly related to features seen in the distribution functions in Fig. 4. The peak in spectra corresponds to beam-like features seen in the ion distribution functions. Also, the high degree of anisotropy is associated with strong gradients in phase space density. In some cases there appears to be three components to the plasma: an energetic component sampled by the SST that has a power law spectrum, a lower energy component (possibly exponential), and beam-like features superposed on the other two components. Also notice that the directionality of ion fluxes appears more organized by the earthward-tailward direction than by the direction of the magnetic field. As is noted in Fig. 4, the magnetic elevation angle for the last two distributions on 26 July 1997, is about  $40^\circ$  and  $85^\circ$ , respectively. For the second and third distributions on 27 March 1996, the elevation angle is about  $30^\circ$  and  $90^\circ$ . Even though there are large changes in the direction of the magnetic field, the highest intensity fluxes are directed earthward in all four cases. Finally, note that the peak of the spectra in the fifth row lies at the high end of the energy detection threshold ( $\sim 30$  keV) of the ion electrostatic analyzer. This incomplete sampling of the ion population indicates that the velocity moments calculated from the distribution function under represents the actual values of the real population.

The second row shows electron spectra coincident with the ion spectra in the first row. There are low and high energy components present in both spectra. The SST shows the continuation of the high energy component. Compared to the spectrum from 05:36 on 26 July 1997, the spectrum from 09:07 on 27 March 1996, has lower fluxes at lower energies and higher fluxes at energies greater than a few keV. Also, at the lowest energies there is evidence of bidirectional pitch-angle anisotropy which may be indicative of previous activity.<sup>13</sup> In the fourth row, we see a very dynamic spectrum on 26 July 1997. The spectrum appears to be in the process of evolving from a spectrum of the type seen at 05:36 to a spectrum similar to that seen at 06:02. The low energy fluxes are decreasing as the higher energy fluxes are increasing. The

dividing energy between the two regimes is  $\sim 3$  keV, where the fluxes remain approximately constant. The spacecraft is most likely to be in the acceleration region and fortuitously captured the evolution during the 3 s integration. At 10:30 on 27 March 1996, the spectrum still contains a large flux of lower energy electrons and a relatively low flux of high energy electrons. This is unexpected given the dynamic, anisotropic ion spectrum at the same time. There are two possible explanations for these different spectra. The first may be timing. The ion spectrum is integrated over 50 s while the electron spectrum is only integrated over the first 3 s. Perhaps the plasma became more dynamic after the first 3 s. Alternatively, it could be a finite gyroradius effect which would have implications for the scale sizes of dynamic regions and spatial gradients within the plasma sheet. With a local magnetic field of 20 nT, a proton of 1 keV energy has a gyroradius greater than 200 km. The gyroradius of a 1 keV electron is only about 5 km. The spacecraft could be in a cool region of plasma sampling the local electrons. Ions from a hotter region of plasma a few hundred kilometers away may be entering the detector contributing to the dynamic, anisotropic ion distribution. In the last row, we see electron spectra commonly observed in conjunction with dynamic ion spectra. These spectra contain relatively depressed low energy fluxes, a peak at a few keV, and elevated fluxes at higher energies compared to quiet time plasma sheet electron spectra.

### III. SUMMARY AND CONCLUSIONS

We have shown through a comparison of global auroral images and plasma sheet ion and magnetic field observations that plasma sheet dynamics is closely related to auroral activity through a large range of scale sizes from small pseudo-breakups to global expansive phase aurorae. The character of the plasma sheet dynamics during these two types of auroral activity is very similar. In both intervals studied here, high earthward ion velocity moments, large amplitude, high frequency magnetic field fluctuations coincident with large  $\langle \mathbf{v} \rangle$ , and ions and electrons energized up to MeV energies were observed in the plasma sheet.

The ion phase space distributions during the high  $\langle \mathbf{v} \rangle$  events are highly anisotropic with possibly nongyrotropic beam-like features present. The distributions also appear to be multicomponent with lower energies (less than  $\sim$  few keV) behaving dynamically differently from higher energy ions. There is no simple transformation to a frame in which the distributions will appear symmetric. In view of the multicomponent plasma population and the dynamic nature of the plasma, describing the behavior in terms of fluid moments will not yield a complete picture of plasma dynamics. A kinetic description is needed.

The distributions are very likely to be revealing only an average picture of ion dynamics. This is because the number of ion gyroperiods during integration varies from about 15 for 50 s integrations to about 5 for 25 s integrations for the magnitudes of  $\mathbf{B}$  observed. Also during the integration, the magnetic field is rapidly fluctuating, and the average direction of  $\mathbf{B}$  is used to plot the distribution functions. During

these fluctuations, the spacecraft may be sampling different regions of the magnetotail plasma, and spatial and temporal effects could be mixed. Another possible explanation for the asymmetric distributions is strong particle gradients. Strong particle gradients in the  $\mathbf{v} \times \mathbf{B}$  direction, i.e.,  $-Y$  direction, can result in a mean velocity in the earthward direction. Finally, inductive electric fields due to the time variations of the magnetic field will alter the plasma distributions.

The ion energy spectra show that there is efficient ion energization up to MeV energies during large  $\langle \mathbf{v} \rangle$  events. Also the anisotropy in fluxes seen at energies below 30 keV persists to the highest energy channels. The consistent earthward-tailward directionality of ion anisotropy implies that the ions are not responding exclusively to local magnetic field effects. It is possible that the ions in these events are nonmagnetized, although the local  $\beta$  of the plasma for these anisotropic spectra is between 0.4 and 0.8. The magnetic field may also be changing in direction or magnitude over scale sizes of the ion gyroradius, hundreds of km for keV ions in the plasma sheet. The locally measured magnetic field may not be representative of the magnetic field that the ions encounter during a significant fraction of their orbits. Inductive electric fields and time changes in inductive electric fields will additionally influence particle dynamics. Finally, in order to do a detailed analysis of ion dynamics, it is necessary to remove convective effects by transforming into the proper frame of reference. This is more important for lower energy plasma (less than  $\sim 1$  keV) where the thermal velocities may be on the order of or less than the convective velocity. This has not been taken into account in the present study, but will be included in future studies.

Recently there have been reports of earthward traveling field-aligned MeV ions observed by the Interball spacecraft at auroral latitudes at altitudes of  $3 R_E$ .<sup>14</sup> These ions may be directly linked to increases in MeV ion fluxes measured by Wind at  $\sim 10$  to  $15 R_E$  distances.

Electron energy spectra indicate that the electron population changes in association with large ion  $\langle \mathbf{v} \rangle$ . During and after these events, electron fluxes at energies below a few keV decrease while fluxes at energies above a few keV to MeV energies increase. This indicates that the spacecraft is sampling a new population of electrons.

Previous studies relating auroral activity to plasma sheet parameters relied on a MHD fluid description of plasma sheet dynamics.<sup>7,15</sup> Examination of kinetic features shows additional details not indicated in the fluid description, and a different picture is obtained of the dynamics. The physical mechanism which is responsible for the dynamic processes leading to the large ion velocity moments is still unknown and requires further study. Future studies will examine the

detailed plasma distributions to separate adiabatic and non-adiabatic features to better identify the acceleration processes involved in the plasma sheet.

The similarity of the plasma sheet dynamics is in contrast to the difference in the auroral activity for these two intervals. The only apparent difference between these events is the size of the region of intense auroral emission. What controls the scale size and intensity of energetic electron precipitation into the ionosphere? Since the physics of both events look similar in the plasma sheet, the question arises whether there is a distinction between pseudobreakups and substorm expansive phase aurorae.

## ACKNOWLEDGMENTS

The Wind magnetometer data are courtesy of Ronald P. Lepping.

This work was supported in part by NASA Grant Nos. NAG5-3170 and NAG5-26580.

<sup>1</sup>C. T. Elvey, Proc. Natl. Acad. Sci. U.S.A. **43**, 63 (1957).

<sup>2</sup>S.-I. Akasofu, Planet. Space Sci. **12**, 273 (1964).

<sup>3</sup>M. R. Torr, D. G. Torr, M. Zukic, R. B. Johnson, J. Ajello, P. Banks, K. Clark, K. Cole, C. Keffer, G. Parks, B. Tsurutani, and J. Spann, Space Sci. Rev. **71**, 329 (1995).

<sup>4</sup>R. P. Lin, K. A. Anderson, S. Ashford, C. Carlson, D. Curtis, R. Ergun, D. Larson, J. McFadden, M. McCarthy, G. K. Parks, H. Rème, J. M. Bosqued, J. Coutelier, F. Cotin, C. D'uston, K.-P. Wenzel, T. R. Sanderson, J. Henrion, J. C. Ronnet, and G. Paschmann, Space Sci. Rev. **71**, 125 (1995).

<sup>5</sup>R. P. Lepping, M. H. Acuña, L. F. Burlaga, W. M. Farrell, J. A. Slavin, K. H. Schatten, F. Mariani, N. F. Ness, F. M. Neubauer, Y. C. Whang, J. B. Byrnes, R. S. Kennon, P. V. Panetta, J. Scheifele, and E. M. Worley, Space Sci. Rev. **71**, 207 (1995).

<sup>6</sup>M. O. Fillingim, G. K. Parks, L. J. Chen, M. Brittner, G. A. Germany, J. F. Spann, D. Larson, and R. P. Lin, Geophys. Res. Lett. **27**, 1379 (2000).

<sup>7</sup>V. Angelopoulos, T. D. Phan, D. E. Larson, F. S. Mozer, R. P. Lin, K. Tsuruda, H. Hayakawa, T. Mukai, S. Kokubun, T. Yamamoto, D. J. Williams, R. W. McEntire, R. P. Lepping, G. K. Parks, M. Brittner, G. Germany, J. Spann, H. J. Singer, and K. Yumoto, Geophys. Res. Lett. **24**, 2271 (1997).

<sup>8</sup>L. J. Chen, G. K. Parks, M. McCarthy, D. Larson, and R. P. Lin, Geophys. Res. Lett. **27**, 1847 (2000).

<sup>9</sup>D. Lummerzheim and J. Lilensten, Ann. Geophys. (Germany) **12**, 1039 (1994).

<sup>10</sup>G. A. Germany, G. K. Parks, M. Brittner, J. Cumnock, D. Lummerzheim, J. F. Spann, L. Chen, P. G. Richards, and F. J. Rich, Geophys. Res. Lett. **24**, 995 (1997).

<sup>11</sup>N. A. Tsyganenko, Planet. Space Sci. **37**, 5 (1989).

<sup>12</sup>V. Angelopoulos, W. Baumjohann, C. F. Kennel, F. V. Coroniti, M. G. Kivelson, R. Pellat, R. J. Walker, H. Lühr, and G. Paschmann, J. Geophys. Res., [Space Phys.] **97**, 4027 (1992).

<sup>13</sup>L. J. Chen, D. Larson, R. P. Lin, M. McCarthy, and G. K. Parks, Geophys. Res. Lett. **27**, 843 (2000).

<sup>14</sup>V. N. Lutsenko (private communication, 2000).

<sup>15</sup>D. H. Fairfield, T. Mukai, M. Brittner, G. D. Reeves, S. Kokubun, G. K. Parks, T. Nagai, H. Matsumoto, K. Hashimoto, D. A. Gurnett, and T. Yamamoto, J. Geophys. Res., [Space Phys.] **104**, 355 (1999).